university of groningen

University Medical Center Groningen

University of Groningen

The sloan lens acs survey. II. Stellar populations and internal structure of early-type lens galaxies

Treu, Tommaso; Koopmans, Léon V.; Bolton, Adam S.; Burles, Scott; Moustakas, Leonidas A.

Published in:
Astrophysical Journal

IMPORTANT NOTE: You are advised to consult the publisher's version (publisher's PDF) if you wish to cite from it. Please check the document version below.

Document Version
Publisher's PDF, also known as Version of record

Publication date:
2006

Link to publication in University of Groningen/UMCG research database

Citation for published version (APA):
Treu, T., Koopmans, L. V., Bolton, A. S., Burles, S., & Moustakas, L. A. (2006). The sloan lens acs survey. II. Stellar populations and internal structure of early-type lens galaxies. *Astrophysical Journal*, *640*(2), 662-672. http://adsabs.harvard.edu/abs/2006ApJ...640..662T

Copyright
Other than for strictly personal use, it is not permitted to download or to forward/distribute the text or part of it without the consent of the author(s) and/or copyright holder(s), unless the work is under an open content license (like Creative Commons).

The publication may also be distributed here under the terms of Article 25fa of the Dutch Copyright Act, indicated by the “Taverne” license. More information can be found on the University of Groningen website: https://www.rug.nl/library/open-access/self-archiving-pure/taverne-amendment.

Take-down policy
If you believe that this document breaches copyright please contact us providing details, and we will remove access to the work immediately and investigate your claim.

Downloaded from the University of Groningen/UMCG research database (Pure): http://www.rug.nl/research/portal. For technical reasons the number of authors shown on this cover page is limited to 10 maximum.

The Astrophysical Journal, 640:662–672, 2006 April 1
© 2006. The American Astronomical Society. All rights reserved. Printed in U.S.A.

THE SLOAN LENS ACS SURVEY. II. STELLAR POPULATIONS AND INTERNAL STRUCTURE OF EARLY-TYPE LENS GALAXIES[1]

Tommaso Treu,[2,3] Léon V. Koopmans,[4] Adam S. Bolton,[5,6] Scott Burles,[5] and Leonidas A. Moustakas[7]

Received 2005 August 2; accepted 2005 November 29

ABSTRACT

We use *HST* images to derive effective radii and effective surface brightnesses of 15 early-type (E+S0) lens galaxies identified by the SLACS Survey. Our measurements are combined with stellar velocity dispersions from the SDSS database to investigate for the first time the distribution of lens galaxies in the fundamental plane (FP) space. Accounting for selection effects (top priority to the largest Einstein radii and thus approximately to the largest velocity dispersions, $\sigma \gtrsim 240$ km s^{-1}) and for passive evolution, the distribution of the lens galaxies inside the FP is indistinguishable from that of the parent sample of SDSS galaxies. We conclude that SLACS lenses are a fair sample of high velocity dispersion E+S0s. By comparing the central stellar velocity dispersion (σ) with the velocity dispersion that best fits the lensing models ($\sigma_{\rm SIE}$) we find $\langle f_{\rm SIE}\rangle \equiv \langle \sigma/\sigma_{\rm SIE}\rangle = 1.01 \pm 0.02$ with 0.065 rms scatter. We infer that within the Einstein radii (typically $R_e/2$) the SLACS lenses are very well approximated by isothermal ellipsoids, requiring a fine tuning of the stellar and dark matter distribution (the bulge-halo "conspiracy"). Interpreting the offset from the local FP in terms of evolution of the stellar mass-to-light ratio, we find $d\log(M/L_B)/dz = -0.69 \pm 0.08$ (rms 0.11) consistent with the rate found for field E+S0s and with most of the stars being old ($z_f > 2$) and less than $\sim$10% of the stellar mass having formed below $z = 1$. We discuss our results in the context of formation mechanisms such as collisionless ("dry") mergers.

Subject headings: galaxies: elliptical and lenticular, cD — galaxies: evolution — galaxies: formation — galaxies: structure — gravitational lensing

Online material: color figures

1. INTRODUCTION

The properties of early-type galaxies in the local universe obey several empirical scaling laws, such as the correlation between host velocity dispersion and the mass of the central supermassive black hole (Ferrarese & Merritt 2000; Gebhardt et al. 2000), correlations between velocity dispersion and stellar ages and chemical composition (Bender et al. 1992, 1993), and the correlation between velocity dispersion, effective radius, and effective surface brightness known as the fundamental plane (FP; Djorgovski & Davis 1987; Dressler et al. 1987). Understanding the origin of these scaling laws is a challenge for galaxy formation models, because they imply a degree of homogeneity difficult to explain without invoking a substantial amount of fine-tuning or feedback, which are still unexplained in the hierarchical merging scenario.

In particular, the fundamental plane can be seen as a scaling relation between a galaxy's effective (dynamical) mass and effective (dynamical) mass-to-light ratio (M/L; Faber et al. 1987; Bender et al. 1992; van Albada et al. 1995) in the sense that mass-to-light ratio increases with effective mass (the "tilt" of the FP). This tilt could be due (Ciotti et al. 1996; Pahre 1998; Trujillo et al. 2004; Lanzoni et al. 2004) to trends in stellar populations (more massive galaxies are older and more metal rich), in the distribution of dark matter (more massive galaxies contain more dark matter), or in structural properties (the distribution function depends on mass; e.g., Bertin et al. 2002). The distribution of galaxies along the FP is also nontrivial: galaxies do not occupy the whole plane but live in well-defined zones, avoiding a well-defined region of the plane ("zone of avoidance"). From a theoretical point of view it is difficult to reproduce both the tilt and the distribution of galaxies inside the FP (e.g., Nipoti et al. 2003).

In recent years, several groups have measured the FP of early-type galaxies at cosmological redshift (van Dokkum & Franx 1996; Kelson et al. 1997; Pahre 1998; Bender et al. 1998; van Dokkum et al. 1998, 2001; Treu et al. 1999, 2001a, 2001b, 2002, 2005a, 2005b; Kelson et al. 2000; van Dokkum & Ellis 2003; Gebhardt et al. 2003; van Dokkum & Stanford 2003; van der Wel et al. 2004, 2005; Wuyts et al. 2004; Fritz et al. 2005; Holden et al. 2005; di Serego Alighieri et al. 2005; Moran et al. 2005) to measure the evolution of their M/L and hence constrain their star formation history. The results of these studies can be summarized as follows: massive early-type galaxies (greater than $10^{11.5}\,M_\odot$) appear to be evolving slowly below $z \sim 1$, consistent with the passive evolution of an old stellar population formed at $z > 2$. At smaller masses, signs of recent star formation start to appear first in the field (at $z \sim 0.5$; Treu et al. 2002, 2005b; van der Wel et al. 2005) and at higher redshifts

[1] Based on observations made with the NASA/ESA *Hubble Space Telescope*, obtained at the Space Telescope Science Institute (STScI), which is operated by the Association of Universities for Research in Astronomy (AURA), Inc., under NASA contract NAS5-26555. These observations are associated with program 10174. Support for program 10174 was provided by NASA through a grant from STScI, which is operated by the AURA, Inc., under NASA contract NAS5-26555.

[2] Department of Physics, University of California, Santa Barbara, CA 93106; tt@physics.ucsb.edu.

[3] Department of Physics and Astronomy, UCLA, Box 951547, Knudsen Hall, Los Angeles, CA 90095.

[4] Kapteyn Institute, P.O. Box 800, 9700AV Groningen, Netherlands; koopmans@astro.rug.nl.

[5] Department of Physics and Kavli Institute for Astrophysics and Space Research, Massachusetts Institute of Technology, 77 Massachusetts Avenue, Cambridge, MA 02139; bolton@alum.mit.edu, burles@mit.edu.

[6] Harvard-Smithsonian Center for Astrophysics, 60 Garden Street, Cambridge, MA 02138; abolton@cfa.harvard.edu.

[7] Jet Propulsion Laboratory, Mail Stop 169-327, California Institute of Technology, Pasadena CA 91109; leonidas@jpl.nasa.gov.

possibly even in clusters (Holden et al. 2005). Mass seems to be the dominant parameter determining the star formation history, while environment affects M/L only to a lesser degree (Moran et al. 2005; Yee et al. 2005). This trend is consistent with the *downsizing* scenario (i.e., star formation activity moves to lower masses from high to low redshift; Cowie et al. 1996) seen in a number of studies (e.g., McIntosh et al. 2005; Treu et al. 2005a; Juneau et al. 2005; see de Lucia et al. 2006 for a theoretical point of view; see Gavazzi 1993 for a discussion of downsizing ante litteram for disk galaxies, based on fossil evidence). In the case of early-type galaxies, the concept of downsizing refers to the fact that stars are oldest in the most massive systems.

Little is known about scaling relations of early-type lens galaxies. Do they follow the same scaling laws of normal early-type galaxies? In principle, anomalous structural properties—such as an unusually high concentration/mass density—or mass from a large-scale structure (e.g., a group or a filament) projected along the line of sight could boost lensing efficiency and therefore a lensing-selected sample could be biased. Based on the limited amount of information available so far, no significant difference has been found between the structural properties (e.g., Treu & Koopmans 2004) of lens and nonlens galaxies, supporting the hypothesis that E+S0 lenses are representative of the whole E+S0 population.

In this paper, we exploit the large and homogeneously selected sample of lenses identified in a relatively narrow redshift range by the Sloan Lenses ACS Survey (SLACS; Bolton et al. 2005, 2006, hereafter Paper I),[8] to study in detail the fundamental plane of lens galaxies, both in terms of tilt and distribution of galaxies along the plane. We quantify the degree of homogeneity of the early-type galaxies by measuring the ratio between stellar velocity dispersion and velocity dispersion of the singular isothermal ellipsoid (SIE) mass model that best fits the geometry of the multiple images, using the results of the lens models derived by Koopmans et al. (2005; hereafter Paper III).

In addition, we use the sample to study the evolution of the FP of lens galaxies with redshift as a diagnostic of their stellar populations. Previous studies on this topic have reached discordant conclusions. In a pioneering work, Kochanek et al. (2000; see also Rusin et al. 2003) assumed isothermal mass density profiles (see Rusin & Kochanek 2005 for a more general approach) to convert image separations into velocity dispersion and construct the FP of early-type lens galaxies without stellar velocity dispersion information all the way out to $z \sim 1$, finding relatively slow evolution of their M/L [$d \log (M/L_B)/dz = -0.56 \pm 0.04$] at variance with the faster evolution measured by direct determinations of the stellar velocity dispersions (e.g., $-0.72^{+0.07}_{-0.05} \pm 0.04$, Treu et al. 2005b; -0.76 ± 0.07, van der Wel et al. 2005).

Other than a genuine intrinsic difference in the stellar populations, the origin of this discrepancy could be attributed to departures from isothermality, to environmental effects, to differences in the analysis and fitting techniques [e.g., van de Ven et al. 2003 reanalyzed the Rusin et al. sample, obtaining faster evolution $d \log (M/L_B)/dz = -0.62 \pm 0.13$]. Or else, the difference could be understood in terms of downsizing. In fact—as a result of the shape of the luminosity function of early-type galaxies and the scaling of lensing cross section with mass—lens samples tend include mostly massive early-type galaxies ($\sigma \sim 250$ km s^{-1}) as opposed to luminosity-selected samples, which tend to be dominated by galaxies close to the limiting magnitude.

Early results on the distribution of mass and light in E+S0 lenses were obtained by the Lens Structure and Dynamics (LSD) Survey (Koopmans & Treu 2002, 2003; Treu & Koopmans 2002a, 2002b, 2003, 2004; hereafter collectively KT), which published stellar velocity dispersions for five lenses in the redshift range $z \approx 0.5$–1. KT found that the image separation under isothermal assumptions provided a good approximation for stellar velocity dispersion and that the evolution of the stellar M/L was in good agreement with that measured for nonlens samples, albeit with large error bars because of the small sample size. The SLACS sample is the largest sample of lenses to date with measured stellar velocity dispersions. It is therefore ideally suited to be combined with the LSD sample to investigate with higher precision any difference in the stellar populations of lens and nonlens early-type galaxies, bearing in mind the SLACS selection process (luminous red galaxies and/or quiescent spectra, H$\alpha < 1.5$ Å; see Paper I and § 2).

The plan of the paper follows. Section 2 presents the sample and the data. Section 3 investigates the internal structure and homogeneity of SLACS lenses using the FP as a diagnostic tool. Section 4 describes the redshift evolution of the FP of the combined SLACS+LSD sample and compares it to that of nonlens early-type galaxies. Section 5 summarizes our results. As in the rest of this series, we adopt Vega magnitudes and a cosmological model with $\Omega_m = 0.3$, $\Omega_\Lambda = 0.7$, and $H_0 = 70\, h_{70}$ km s^{-1} Mpc^{-1} (with $h_{70} = 1$ when needed).

2. SAMPLE SELECTION AND DATA ANALYSIS

The sample analyzed in this paper is composed of the E+S0 lens galaxies without bright nearby companions identified by SLACS as of 2005 March 31—the cutoff line for this first series of papers. A full description of SLACS and the selection process—together with images and spectra of all the lenses—is given in Paper I of this series (see also Bolton et al. 2004, 2005).[9] For easy reference, we give here a brief summary. First, lens candidates are found in the SDSS database by identifying composite spectra made of a quiescent stellar population and multiple emission lines at a higher redshift (see Bolton et al. 2004). The spectra are taken from the luminous red galaxies sample (Eisenstein et al. 2001) and the main galaxy sample (Strauss et al. 2002). Quiescent spectra are selected from the main sample by imposing a limit of H$\alpha < 1.5$ Å on the equivalent width.

Second, the probability of the candidate being a lens, as opposed to a chance overlap within the fiber, is computed based on the SDSS stellar velocity dispersion, the lens and source redshifts, and an isothermal mass model. In this model, the probability of being a lens is a monotonically increasing function of Einstein radius and, therefore, for any given source and lens redshift, of velocity dispersion.

Third, the most promising candidates are followed up with ACS on on the *Hubble Space Telescope* (*HST*) in snapshot mode (420 s exposures through filters F435W and F814W) to confirm the lens hypothesis. The initial candidate list for this proposal consisted of 117 galaxies. The 49 candidates with the largest Einstein radius ended up in the Snapshot target list.

In order to facilitate comparison with nonlens sample it is useful to express our selection criterion—at least approximately—in terms of velocity dispersion instead of Einstein radius. In general, the Einstein radius depends also on the angular distance between the lens and the source (D_{ls}) and between us and the source (D_s), since $R_{\rm Einst} \propto (D_{ls}/D_s)\sigma^2$. However, the range in source and lens redshifts is relatively small for our sample,

[8] See http://www.slacs.org.

[9] See also the SLACS Web site at http://www.slacs.org.

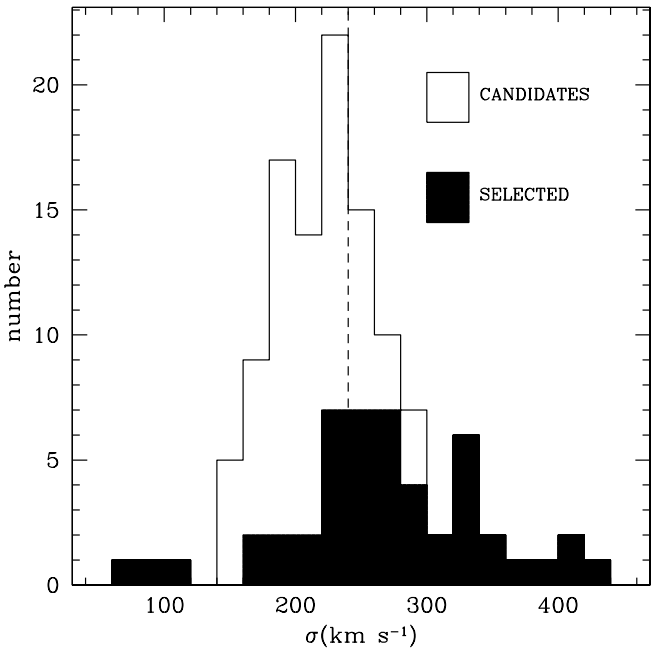

FIG. 1.—Distribution of velocity dispersion for the parent candidate list and for the 49 targets of the *HST* Snapshot program. The selection in Einstein radius picks out the galaxies with the largest velocity dispersion. The vertical dashed line represents the expected threshold for a velocity dispersion–limited sample of 49 objects.

and therefore the angular distance ratio is almost constant $\langle D_{ls}/D_s \rangle = 0.58$, with an rms scatter of 0.15. For this reason and because of the dependency of the Einstein radius on σ^2, velocity dispersion is by far the dominant parameter for selection, with lens and source redshift being a minor second-order effect. This is illustrated in Figure 1, in which we show the distribution of velocity dispersion for the full list of 117 candidates and the subsample of 49 in the *HST* target list. A vertical dashed line indicates the threshold that would be expected for a purely velocity dispersion selected sample (i.e., the top 42%, or 49/117, of velocity dispersions). Although the angular distances ratio softens the cutoff, to first approximation we can say our sample should be representative of high velocity dispersion early-type galaxies ($\sigma \gtrsim 240$ km s^{-1}).

As part of our ongoing effort, we successfully proposed a second more extensive Snapshot program in Cycle 14 (118 targets; GO-10587; PI: A. S. Bolton). The target list for the Cycle 14 program is designed to provide a uniform distribution of lens velocity dispersions, and therefore the number of targets increases with decreasing velocity dispersion to compensate the declining lensing probability. When completed, the Cycle 14 survey will allow us to extend our investigation to early-type galaxies with a larger range of velocity dispersions.

In our treatment of selection effects in § 3.1, we construct control samples with exactly the same distribution of σ. However, we also model our selection process primarily as a fixed threshold in σ, which has the double benefit of being simple and redshift independent, and of being useful for comparisons with samples of nonlenses. We show that this approximate selection procedure applied to the control samples, also reproduces the observed properties of the SLACS lenses.

Of the 19 lenses confirmed so far, 4 are not considered in this paper: 1 lens is rejected because it is a spiral galaxy, and the other 3 are rejected because they are double lenses or have bright companions within the SDSS fiber.

Surface photometry was obtained for all the 15 single-lens galaxies characterized by early-type morphology (i.e., E or S0; listed in Table 1) by fitting de Vaucouleurs profiles to the ACS images using `galfit` (Peng et al. 2002). Lensed features, as well as neighboring galaxies, were carefully masked out during the fit to minimize contamination.

A TinyTim (Krist 2005) generated point-spread function (PSF) was used to convolve the models. The resulting structural parameters—effective radius (r_e and R_e, respectively, in arcseconds and kiloparsecs) and effective surface brightness (SB_e)—are fairly insensitive to the choice of PSF, as expected because the effective radii are typically much larger ($2''$–$3''$) than the half-width half-maximum of the PSF ($\sim 0''.05$). The uncertainty on the structural parameters was estimated by repeating the two-dimensional fits after varying the sky levels by twice its standard deviation. As commonly known (e.g., Hamabe & Kormendy 1987; Jørgensen et al. 1993; Treu et al. 2001b), uncertainties on the effective radius and effective surface brightness

TABLE 1
SUMMARY OF RELEVANT MEASUREMENTS

SDSS ID	z	σ_{ap}	m_8	r_{e8}	m_4	r_{e4}
J003753.21−094220.1.....	0.1954	265 ± 10	15.75 ± 0.01	2.54 ± 0.02	18.85 ± 0.03	2.71 ± 0.07
J021652.54−081345.3.....	0.3317	332 ± 23	16.29 ± 0.05	3.51 ± 0.22	19.74 ± 0.10	3.69 ± 0.37
J073728.45+321618.5.....	0.3223	310 ± 15	16.47 ± 0.03	3.28 ± 0.13	19.92 ± 0.04	3.25 ± 0.12
J091205.30+002901.1.....	0.1642	313 ± 12	15.03 ± 0.00	4.80 ± 0.02	17.92 ± 0.03	5.64 ± 0.17
J095629.77+510006.6.....	0.2405	299 ± 16	16.18 ± 0.01	2.65 ± 0.03	19.58 ± 0.06	2.24 ± 0.14
J095944.07+041017.0.....	0.1260	212 ± 12	16.34 ± 0.02	1.82 ± 0.05	19.11 ± 0.01	2.15 ± 0.02
J125028.25+052349.0.....	0.2318	254 ± 14	16.22 ± 0.00	1.78 ± 0.01	19.53 ± 0.02	1.45 ± 0.02
J133045.53−014841.6.....	0.0808	178 ± 9	16.51 ± 0.00	1.23 ± 0.01	18.99 ± 0.01	1.41 ± 0.02
J140228.21+632133.5.....	0.2046	275 ± 15	15.84 ± 0.00	3.12 ± 0.02	19.37 ± 0.08	2.33 ± 0.20
J142015.85+601914.8.....	0.0629	194 ± 5	14.63 ± 0.03	2.63 ± 0.10	17.13 ± 0.02	2.57 ± 0.05
J162746.44−005357.5.....	0.2076	275 ± 12	16.27 ± 0.01	2.15 ± 0.02	19.71 ± 0.02	1.71 ± 0.03
J163028.15+452036.2.....	0.2479	260 ± 16	16.34 ± 0.01	2.09 ± 0.02	19.79 ± 0.13	2.16 ± 0.31
J230053.14+002237.9.....	0.2285	283 ± 18	16.57 ± 0.01	1.88 ± 0.01	20.05 ± 0.05	1.70 ± 0.09
J230321.72+142217.9.....	0.1553	260 ± 15	15.23 ± 0.01	4.24 ± 0.04	18.21 ± 0.05	4.32 ± 0.19
J232120.93−093910.2.....	0.0819	236 ± 7	14.19 ± 0.00	4.49 ± 0.01	16.74 ± 0.01	5.58 ± 0.08

NOTES.—For each SLACS lens (see coordinates and SDSS photometry in Paper I) we list redshift, SDSS velocity dispersion, and *HST* magnitude and effective radius through the F814W and F435W filters (magnitudes are in the Vega system, corrected for Galactic extinction; effective radii are in arcseconds).

TABLE 2
Summary of Relevant Corrected Quantities

SDSS ID	σ	$\sigma_{\rm SIE}$	$SB_{e,V}$	$R_{e,V}$	V	$SB_{e,B}$	$R_{e,B}$	B
J003753.21−094220.10.....	295 ± 13	271	20.01 ± 0.06	6.68 ± 0.06	−22.68	20.79 ± 0.10	6.13 ± 0.09	−21.71
J021652.54−081345.30.....	325 ± 12	344	20.99 ± 0.06	14.66 ± 0.23	−23.41	21.97 ± 0.16	15.49 ± 0.39	−22.55
J073728.45+321618.50.....	326 ± 16	297	20.80 ± 0.19	15.32 ± 0.46	−23.69	21.65 ± 0.19	15.27 ± 0.42	−22.84
J091205.30+002901.10.....	229 ± 13	217	20.39 ± 0.11	4.50 ± 0.05	−21.45	21.37 ± 0.05	4.75 ± 0.03	−20.58
J095629.77+510006.60.....	290 ± 16	298	20.36 ± 0.09	9.35 ± 0.29	−23.06	21.11 ± 0.42	8.39 ± 0.53	−22.08
J095944.07+041017.00.....	279 ± 17	314	20.06 ± 0.16	8.23 ± 0.44	−23.09	21.01 ± 0.69	8.34 ± 0.89	−22.17
J125028.25+052349.00.....	245 ± 7	257	20.48 ± 0.03	7.93 ± 0.07	−22.59	21.49 ± 0.08	8.47 ± 0.11	−21.72
J133045.53−014841.60.....	282 ± 11	279	20.10 ± 0.06	8.48 ± 0.11	−23.11	21.01 ± 0.15	8.67 ± 0.19	−22.25
J140228.21+632133.50.....	349 ± 24	346	20.78 ± 0.32	16.95 ± 0.92	−23.94	21.69 ± 0.48	17.28 ± 1.20	−23.06
J142015.85+601914.80.....	305 ± 19	301	20.05 ± 0.07	6.63 ± 0.13	−22.62	20.94 ± 0.26	6.38 ± 0.24	−21.66
J162746.44−005357.50.....	271 ± 16	291	20.85 ± 0.09	11.53 ± 0.26	−23.03	21.78 ± 0.24	11.60 ± 0.44	−22.11
J163028.15+452036.20.....	206 ± 5	204	19.55 ± 0.16	3.15 ± 0.06	−21.51	20.43 ± 0.11	3.13 ± 0.06	−20.62
J230053.14+002237.90.....	274 ± 15	246	19.45 ± 0.03	6.13 ± 0.04	−23.05	20.19 ± 0.09	5.68 ± 0.06	−22.15
J230321.72+142217.90.....	318 ± 17	317	20.28 ± 0.09	9.49 ± 0.22	−23.17	21.06 ± 0.31	8.92 ± 0.41	−22.26
J232120.93−093910.20.....	195 ± 10	185	19.86 ± 0.05	2.04 ± 0.02	−20.25	20.80 ± 0.09	2.13 ± 0.03	−19.40

Notes.—For each SLACS lens, as in Table 1, we list central velocity dispersion (in km s^{-1}), velocity dispersion of the best fitting singular isothermal ellipsoid, surface brightness, effective radius, and absolute magnitude in the B- and V-band rest frame (in mag $arcsec^{-2}$ and kpc, respectively). Uncertainties on the absolute magnitude are equal to the uncertainties on the observed magnitudes, plus approximately ∼0.05 mag to account for the K color correction.

are correlated, so that the combination of parameters that enters the fundamental plane ($FP_{\rm ph} = \log R_e - 0.32SB_e$) is very robustly determined. Typical errors on $FP_{\rm ph}$ are ∼0.02–0.03.

Zero points from the latest spectrophotometric calibration of Vega were adopted (Bohlin & Gilliland 2004). Magnitudes were corrected for Galactic extinction using the SDSS $E(B-V)$ values and the coefficients $A_{\rm F435W} = 4.325E(B-V)$ and $A_{\rm F814W} = 1.984E(B-V)$. Observed radii and magnitudes were transformed into rest-frame radii and surface brightness, as described in Treu et al. (2001a). As an independent check of our surface photometry and color transformations, we used publicly available code (Blanton et al. 2003) to compute absolute magnitudes from the SDSS model photometry, finding excellent agreement (e.g., the difference in absolute B magnitude is less than 0.05 with an rms scatter of 0.15), considering the differences in spatial resolution and filter system between *HST* and SDSS.

Stellar velocity dispersions were obtained from the SDSS database. The measured velocity dispersion within the 3″ diameter SDSS fiber $\sigma_{\rm ap}$ was corrected to a standard central velocity dispersion (i.e., measured within $r_e/8$) using the method described by Jørgensen et al. [1995, i.e., $\sigma = \sigma_{\rm ap}(r_e/8\times 1\farcs5)^{-0.04}$]. Relevant spectrophotometric parameters are listed in Tables 1 and 2.

3. THE INTERNAL STRUCTURE OF LENS GALAXIES

In this section, we investigate the internal structure of lens galaxies by studying their location in the FP-space (§ 3.1), and the ratio between stellar velocity dispersion and velocity dispersion of the best-fitting singular isothermal ellipsoid as a diagnostic of the mass profile (§ 3.2).

3.1. *The Fundamental Plane of Lens Galaxies*

The fundamental plane is defined as

$$\log R_e = \alpha \log \sigma + \beta SB_e + \gamma_{\rm FP} \qquad (1)$$

(σ in km s^{-1}, R_e in kiloparsecs, SB_e in mag $arcsec^{-2}$). For this study we adopt as the local relationship the FP of the Coma Cluster in the B band ($\alpha = 1.25$, $\beta = 0.32$, and $\gamma_{\rm FP} = -9.04$; Jørgensen et al. 1996, as fitted by Bender et al. 1998). We use Coma as the local reference for both cluster and field to minimize systematic uncertainties related to filter transformations, distance determination, and selection effects (see the discussion in Treu et al. 2001a, 2005b and van der Wel et al. 2005). In the local universe environmental differences are very small (<0.1 mag $arcsec^{-2}$ at fixed velocity dispersion and effective radius; Bernardi et al. 2003) and negligible for the purpose of this paper.

Figure 2 shows the location of the SLACS lens galaxies in the FP-space, together with the local relationship and Coma galaxies compiled from Jørgensen et al. (1992, 1995; hereafter collectively JFK). The SLACS lens galaxies are distributed

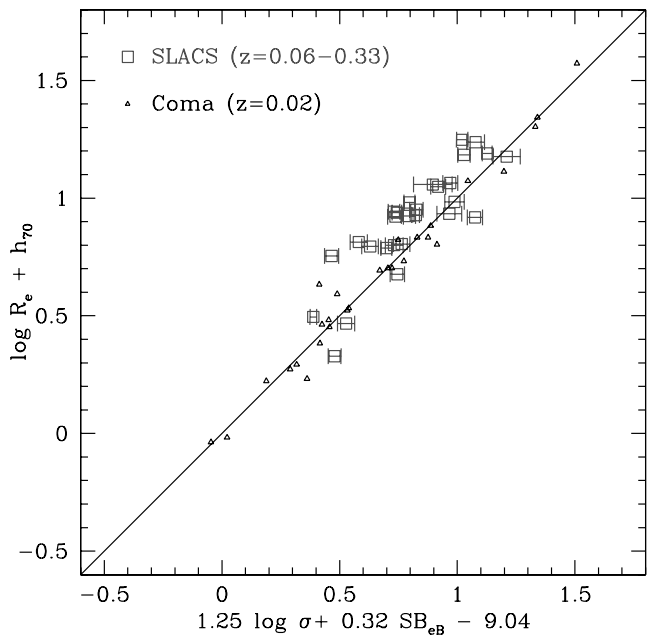

Fig. 2.—Edge-on view of the FP of SLACS E+S0 lens galaxies. Only error bars due to velocity dispersion are shown since the error bars due to surface photometry are highly correlated and move points along the plane. Note that the surface brightness of the SLACS E+S0 galaxies has not been corrected for evolution. The FP of early-type galaxies in the Coma Cluster is shown for comparison (from JFK; *black line and small open triangles*). [*See the electronic edition of the Journal for a color version of this figure.*]

parallel to the local relationship, although on average they are brighter for a given effective radius and central velocity dispersion, as expected because of the higher redshift and the consequently younger stellar populations. Moreover, the rms scatter perpendicular to the FP appears to be larger than that of the Coma sample, because of the relatively large range in redshifts covered by the SLACS sample. As we show in the rest of this section, after correcting for passive evolution, the scatter is consistent with that observed locally.

To proceed further in our analysis of the FP of lens galaxies, let us now consider a particularly useful and insightful parametrization of the FP variables, the so-called κ-space (Bender et al. 1992). The κ-space is obtained by applying the following orthogonal[10] transformation to the FP variables:

$$\kappa_1 = \frac{2\log\sigma + \log R_e}{\sqrt{2}}, \tag{2}$$

$$\kappa_2 = \frac{2\log\sigma + 2\log I_e - \log R_e}{\sqrt{6}}, \tag{3}$$

$$\kappa_3 = \frac{2\log\sigma - \log I_e - \log R_e}{\sqrt{3}}, \tag{4}$$

where I_e is the effective surface brightness in units of $L_\odot$ pc^{-2} [e.g., $\log I_{e,B} = -0.4(\mathrm{SB}_{e,B} - 27)$ in the B band]. The main advantage of this transformation is that κ_1 is proportional to the logarithm of the effective mass ($M = 5\sigma^2 R_e/G$; Bender et al. 1992), while κ_3 is proportional to the logarithm of the effective M/L ($M/L = 5\sigma^2 R_e/G2\pi I_e R_e^2$), and therefore the FP is readily interpreted in terms of physical variables. Furthermore, the plane is viewed almost perfectly edge-on when projected along κ_2 and almost perfectly face-on when projected along κ_3.

To eliminate evolutionary trends in our study of the distribution of SLACS lens galaxies in κ-space, in this section we remove the average evolution found for field early-type galaxies (Treu et al. 2005a, 2005b) as $\log I_{e,B,0} = \log I_{e,B} - 0.72z$ and use $I_{e,B,0}$ in equations (3) and (4). Note that, since the redshifts of the SLACS lens galaxies are relatively small, adopting a different evolutionary rate (e.g., the one from Rusin & Kochanek 2005) would change the position in κ-space by a negligible amount $\sim$0.01–0.02.

The top panel of Figure 3 shows the projection of the SLACS and Coma FP along the κ_2-axis. It is apparent that the SLACS lens galaxies follow the same κ_1-κ_3 relation of Coma galaxies, although they occupy preferably the high κ_1 (i.e., mass) range, as expected, since SLACS lens galaxies are selected to be massive (Paper I). A simple least-square fit gives $\kappa_3 = (0.21 \pm 0.02)(\kappa_1 - 4) + 1.03 \pm 0.01$ for the Coma galaxies and $\kappa_3 = (0.17 \pm 0.07)(\kappa_1 - 4) + 1.03 \pm 0.02$ for the SLACS galaxies. The two fits are consistent within the uncertainties, that are larger for the SLACS sample due to its relatively limited range in κ_1. The scatter of the SLACS sample is 0.060 in κ_3 (0.055 intrinsic after removing in quadrature the average error on κ_3), similar to the local intrinsic scatter of 0.05 reported by Bender et al. (1992).

Somewhat more surprising is the distribution along the FP, i.e., in the κ_1-κ_2–plane, shown in the bottom panel of Figure 3. The SLACS lenses cluster at the edge of the region normally populated by early-type galaxies, concentrating on the border of the zone of avoidance ($\kappa_1 + \kappa_2 = 7.76$; Bender et al. 1992). Thus, although lenses have a normal M/L (κ_3) for a given mass

[10] Considering $2\log\sigma$, $\log I_e$, and $\log R_e$ as original coordinates.

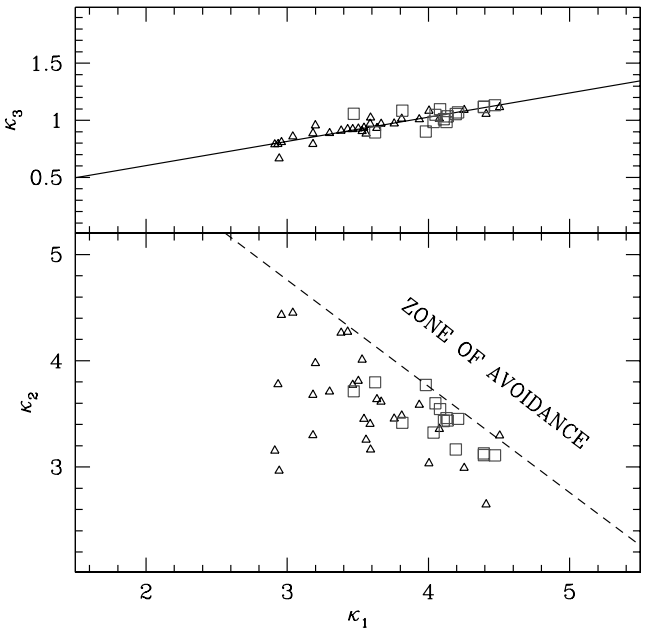

FIG. 3.—Projections of the FP along the so-called κ-space variables ($\kappa_1 \propto \log M, \kappa_2 \propto \log[(M/L_{B,0})I^3_{e,B,0}]$ and $\kappa_3 \propto \log(M/L_{B,0})$). Note that $M/L_{B,0}$ and $I_{e,B,0}$ are the M/L and effective surface brightness corrected to zero redshift according to the evolution measured by Treu et al. (2005b). The top shows the projection on the κ_1-κ_3–plane, corresponding approximately to an edge-on view of the plane. The bottom panel shows the projection on the κ_1-κ_2–plane, corresponding approximately to a face-on view of the plane. SLACS E+S0 lens galaxies are shown as open squares. Early-type galaxies in the Coma Cluster (from JFK; *solid line and small open triangles*) are shown for comparison. The dashed diagonal line represents the border of the zone of avoidance, which is not populated by early-type galaxies (Bender et al. 1992). [*See the electronic edition of the Journal for a color version of this figure*.]

(κ_1; as shown in the top panel of Fig. 3)—and thus occupy the same FP as normal galaxies—they *appear* to have higher κ_2 for a given κ_1. We show in the rest of this section that this is the result of our selection procedure. Taking our selection process into account, lens galaxies are indistinguishable from normal early-type galaxies.

We can quantify any difference between the SLACS lenses and nonlens early-type galaxies by comparing the distribution of distances from the border of the zone of avoidance, i.e., the distribution of $\kappa_1 + \kappa_2 - 7.76$, via the Kolmogorov-Smirnov statistic. A comparison with the JFK Coma sample, limited to $\sigma > 240$ km s^{-1} (§ 2), suggests that the distributions are indistinguishable (47% probability that they follow the same distribution), once selection effects are taken into account. However, this comparison is limited to only five objects and could be affected by differences in the measurement techniques. Therefore, to draw solid conclusions we have to consider a larger and more suitable comparison sample.

The best control sample is provided by the parent population of SDSS selected galaxies. As described in Paper I, for each lens, we can construct a control sample by selecting objects from the same parent sample (luminous red galaxies and the main sample galaxies from the SDSS), with the same redshift and the same limits on the spectroscopic signal-to-noise ratio (S/N) and strength of Hα emission. Since *HST* images are not available for this control sample, we use SDSS photometric and spectroscopic parameters for this comparison, both for the lenses and the nonlenses. Therefore, we can be sure that there is no systematic difference in the measured parameters for the lens sample and the control sample. Moreover, we can avoid uncertainties associated

with K-corrections by making the comparison in the observer's frame κ-space (the o-κ space), where effective radii are expressed in arcseconds and effective surface brightnesses are not corrected to the rest frame. This is possible because the control sample for each lens is chosen to lie in a very thin redshift slice (± 0.005). For each lens we can then compute how o-$\kappa_1 + o$-κ_2 ranks within the distribution for the control objects. If the lenses were a random sample, we would expect the ranks to be uniformly distributed between 0 and 1. In contrast, we find that the lenses typically rank among the largest values of o-$\kappa_1 + o$-κ_2, similarly to what is shown in Figure 3. Thus—not accounting for the selection procedure—the probability that the lenses are drawn from the control sample is as low as 7×10^{-5}.

Most importantly, however, we have to take into account that the SLACS lenses are effectively selected according to velocity dispersion—and we expect this selection to skew our lenses toward large values of κ_1 and κ_2 (see eqs. [2], [3], and [4]). To make a proper comparison, we need to compare the rank of o-$\kappa_1 + o$-κ_2 within the distribution of the parent samples properly selected for Einstein radius. Since for each lens the Einstein radius is only a function of velocity dispersion, it is sufficient to cut each parent sample in velocity dispersion. An important caveat is that the selection in velocity dispersion cannot be applied simply as a symmetric interval around the lens velocity dispersion $\sigma_l \pm N\delta\sigma_l$ (i.e., N times the error on σ_l, as was done in Paper I) but requires a more elaborate procedure. This happens because the lenses are typically on a steeply declining part of the velocity dispersion function, and thus a symmetric interval in σ would overrepresent galaxies with a smaller velocity dispersion. For this reason, we first select galaxies σ in the interval $[\sigma_l, \sigma_l + N\delta\sigma_l]$, and then we select the lower limit, so that the total sample contains as many galaxies above as below σ_l. The one parameter left, N, should be chosen to be the smallest possible that leaves a sizable number of galaxies in each sample; in the analysis we use $N = 0.5$, 1, and 2 to quantify the effects of this choice. The effect of this cut in o-κ–space is illustrated in Figure 4 for a typical system. Selecting objects by velocity dispersion does not significantly alter the edge-on view of the FP (as expected from eqs. [1], [2], [3], and [4]) but picks out only the lenses with the highest o-$\kappa_1 + o$-κ_2 (because lenses typically have the highest velocity dispersion; see § 2). Including this effect, the Kolmogorov-Smirnov statistic gives a probability of 12%, 8%, and 6% that the distribution of distances from the zone of avoidance is the same for the lens and parent samples. In other words, no significant difference is found once selection effects are taken into account.

As an additional check, we also consider our approximate selection in velocity dispersion by limiting the parent sample of each lens to the top 42% velocity dispersions. The effect on each lens is very similar to the one depicted in Figure 4, and the K-S statistic gives a probability of 27% that the lens and control sample are drawn from the same distribution. This confirms that a cut in velocity dispersion is a useful approximation and thus that our lenses are representative of early-type galaxies with $\sigma \gtrsim 240$ km s^{-1}.

The analysis of selection effects in velocity dispersion provides an interesting clue to the interpretation of the zone of avoidance. As shown in Figure 4, a slice in σ is almost parallel to the line delimiting the zone of avoidance (in fact, combining eqs. [1], [2], and [3] yields $\kappa_1 + \kappa_2 = 2.604$, $\log \sigma + 0.577$, and $\log I_e - 0.119$). Therefore, the sharp cutoff observed in the velocity dispersion function of early-type galaxies at $\sigma \sim 350$ km s^{-1} (Sheth et al. 2003) could be one of the dominant factors to explain the existence of the zone of avoidance.

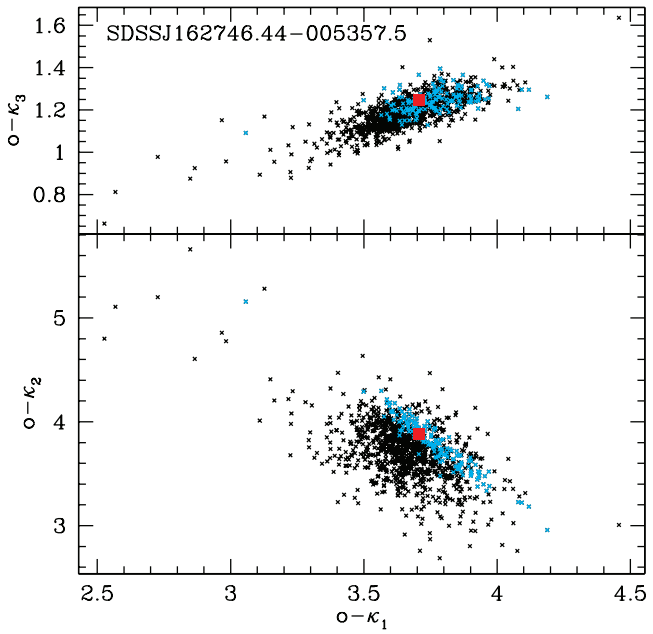

FIG. 4.—Illustration of selection effects in o-κ–space (the equivalent of κ-space in observed quantities; see § 3.1 for details). For a typical case we show the location of the lens (*red filled square*), as well as that of the SDSS control sample (*black and blue crosses*). The top panel shows the projection on the κ_1-κ_3–plane, corresponding approximately to an edge-on view of the fundamental plane. The bottom panel shows the projection on the κ_1-κ_2–plane, corresponding approximately to a face-on view of the plane. Black crosses represent the full SDSS parent sample; blue crosses represent the SDSS subsample selected as our own lens sample (i.e., the top 42% velocity dispersions). Note that our selection procedure tends to select objects in the upper right corner of the (o-κ_1)-(o-κ_2)–plane because both variables are monotonically increasing functions of the velocity dispersion σ.

For completeness, we investigate possible selection effects related to the finite aperture of the SDSS fibers. For example, higher surface brightness galaxies will have a larger fraction of light in the fiber and thus produce higher S/N spectra than galaxies with the same luminosity and larger effective radii. This would make it easier to measure σ, and thus finite fiber effects could be selecting "compact" (i.e., small effective radii for a given luminosity and mass) E+S0 galaxies, which also occupy the top right portion of the κ_1-κ_2–plane (eqs. [3] and [4]). To test this hypothesis, we compared the distribution of spectroscopic S/N's for the lenses to that of the control samples, using the same procedure as above, finding no difference, and thus no evidence that this is a sizable selection bias. Other mechanisms related to the finite fiber size—also weak in magnitude—are discussed in Paper III.

We conclude that SLACS lenses occupy the same FP as high velocity dispersion early-type galaxies. It will be interesting to extend this comparison to lower velocity dispersion galaxies once the Cycle 14 survey is completed.

3.2. *The Homogeneity of Lens Galaxies*

A question of great theoretical and practical import is how close early-type (lens) galaxies are to isothermal density profiles and what is the intrinsic scatter of their total effective mass density profiles. In Paper III these questions are addressed via a joint lensing and dynamical analysis, finding that lenses are extremely close to isothermal ellipsoids, with effective density profiles well approximated by power laws $\rho_{\rm tot} \propto r^{-\gamma'}$, with $\langle \gamma' \rangle = 2.01^{+0.02}_{-0.03} \pm 0.05$ and an intrinsic rms scatter of 0.12 in γ'.

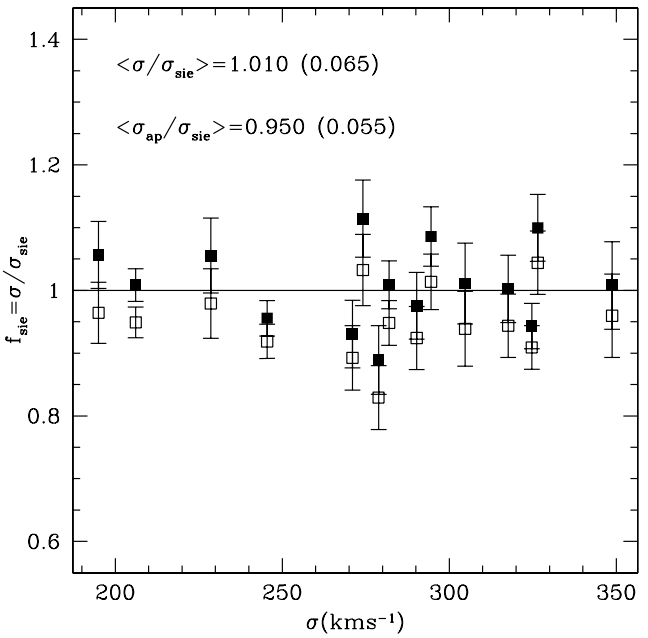

FIG. 5.—Ratio between stellar velocity dispersion and velocity dispersion of the singular isothermal ellipsoid that fits best the lensing geometry. Solid points represent the central velocity dispersion (σ), i.e., corrected to a circular aperture of radius $r_e/8$. Open points represent the stellar velocity dispersion ($\sigma_{\rm ap}$) as measured within the aperture of the SDSS fibers (3″ diameter).

In this paper we take an independent and empirical approach and quantify the homogeneity of early-type galaxies and departures from isothermality by studying the ratio between stellar velocity dispersion and velocity dispersion of the best fitting singular isothermal ellipsoid $\sigma_{\rm SIE}$ (Paper III). The ratio $f_{\rm SIE} = \sigma/\sigma_{\rm SIE}$ is shown in Figure 5. Both the aperture velocity dispersion and the central velocity dispersion agree remarkably well with $\sigma_{\rm SIE}$. In both cases the average ratio is very close to unity ($\langle f_{\rm SIE}\rangle = 1.010 \pm 0.017$ and 0.950 ± 0.015) with a remarkably small scatter (0.065 and 0.055, respectively). No significant correlation is found between $f_{\rm SIE}$ and mass indicators (i.e., σ or κ_1).

From the LSD sample of five higher redshift lenses KT found $\langle f_{\rm SIE}\rangle = 0.87 \pm 0.04$, with an rms scatter of 0.08 (including non-LSD lenses PG1115+080 and B1608+656 raises the average to 0.95 ± 0.07, rms 0.17; Treu & Koopmans 2002b; Koopmans et al. 2003). Although the LSD value is also close to unity, the two measured ratios for LSD and SLACS are only marginally consistent (depending on whether PG1115+080 and B1608+656 are included or not), which is perhaps indicative of significant intrinsic scatter or redshift-dependent average (see Paper III). Similarly, van de Ven et al. (2003) measured the ratio σ/σ_c for a sample of seven lenses (four in common with Treu & Koopmans 2004, plus two additional E+S0 lenses and the bulge of the barred spiral Q2237+030; Huchra et al. 1985). Their parameter σ_c is derived from $\sigma_{\rm SIE}$ by solving the spherical Jeans equation and assuming isothermal total mass distribution and a Hernquist (1990) luminous mass profile. They found $\sigma/\sigma_c = 1.07$, with an rms scatter of 0.27, corresponding to $f_{\rm SIE} = 1.07 \times g$, with $g = 0.9$–1.01 (i.e., $f_{\rm SIE} = 0.96$–1.08) for a range of anisotropy parameters (see van de Ven et al. 2003 for details).

Redshift-dependent effects could be present if contamination from a group/cluster environment or from large-scale structures was an important source of bias. The importance of this effect has been estimated by Keeton & Zabludoff (2004), who analyze mock realizations of groups like PG1115+080 and find that external convergence leads to an overestimate of $\sigma_{\rm SIE}$ by $\sim$6%, with a broad tail extending up to 10%–15% (for additional discussion of environmental effects, see Holder & Schechter 2003, and see Dalal & Watson 2004 for a theoretical point of view; also Fassnacht & Lubin 2002 and Fassnacht et al. 2005 for an observational point of view). In fact, for a fixed velocity dispersion (e.g., 250 km s^{-1}) the Einstein radius in arcseconds is approximately the same (1.″135) for the typical SLACS ($z_l = 0.2$, $z_s = 0.6$) and LSD redshifts ($z_l = 0.5$, $z_s = 2.0$), resulting in a larger Einstein radius in kiloparsecs for LSD lenses (approximately double). Thus, for a large-scale structure of fixed projected density, the mass contribution within the Einstein radius would be $\sim$4 times larger, while the lens mass within the Einstein radius would only grow by a factor of $\sim$2.

Based on the SLACS and LSD samples, we conclude that on average the approximation $\sigma = \sigma_{\rm SIE}$ appears to be working surprisingly well, due perhaps to some as yet unexplained mechanism that couples stellar and dark mass, i.e., a bulge-halo "conspiracy" similar to the disk-halo conspiracy of spiral galaxies. Significant departures are seen, however, in individual cases (up to 11% for SLACS and 30% for LSD+PG 1115+080+B1608+656, including observational errors; see also Kochanek et al. 2006), sufficient to introduce sizable uncertainties in applications that require a precise radial dependency of the mass model (e.g., determination of the Hubble constant from gravitational time delays; note, however, that time delays are sensitive to the slope in the region of the images (Kochanek 2002), while here we are considering the average slope inside the largest of the effective and Einstein radii), as discussed in Paper III.

4. THE EVOLUTION OF THE FUNDAMENTAL PLANE

Under appropriate assumptions (e.g., Treu et al. 2001a, 2005b), the evolution of the fundamental plane can be interpreted as general trends in the luminosity evolution of the stellar populations. If σ and R_e do not evolve with redshift, for an individual galaxy (labeled by the superscript i)

$$\gamma^i_{\rm FP} \equiv \log R^i_e - \alpha \log \sigma^i - \beta {\rm SB}^i_e, \qquad (5)$$

with the offset with respect to the prediction of the FP ($\Delta\gamma^i_{\rm FP} \equiv \gamma^i_{\rm FP} - \gamma_{\rm FP}$) related to the offset of the M/L by

$$\Delta \log(M/L)^i = -\frac{\Delta\gamma^i_{\rm FP}}{2.5\beta}, \qquad (6)$$

which can be used to measure the average evolution and/or scatter of M/L at a given M (see extended discussions in Treu et al. 2001a, 2005b). As is usually done in FP studies, the evolution of the effective M/L can be connected to the star formation history by assuming that $\Delta\log(M/L) = \Delta\log(M_*/L)$ (i.e., stellar mass $M_* \propto M$).

The derived evolution of the effective M/L of SLACS lens galaxies is shown in Figure 6 (*red filled squares*). Although the redshift range covered by the SLACS sample is relatively small, there is a clear indication of evolution, as expected for evolving stellar populations. A simple least-squares fit to the evolutionary rate gives $d\log(M/L_B)/dz = -0.69 \pm 0.08$, with an rms scatter of the residuals of 0.11 in $\Delta\log(M/L_B)$. Including the higher redshift lens galaxies from LSD gives $d\log(M/L_B)/dz = -0.76 \pm 0.03$, leaving unchanged the rms scatter.

For our sample of lenses we can check the effect of adopting $\sigma_{\rm SIE}$ instead of σ in equation (5) (Kochanek et al. 2000). The resulting values of $\Delta\log(M/L_B)$ are plotted as open symbols in Figure 6, showing that in general the change is smaller than

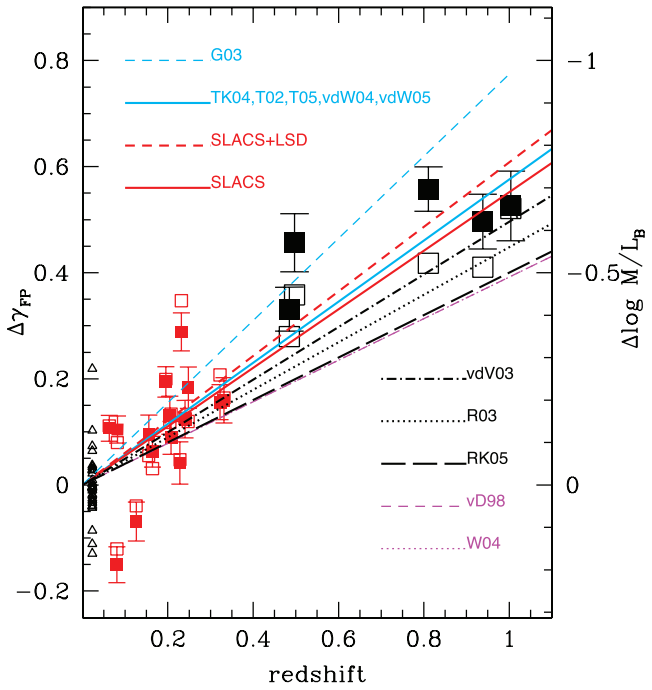

FIG. 6.—Evolution of the effective M/L of early-type galaxies from the evolution of the FP. The small filled (*open*) red squares represent the evolution of SLACS lenses computed using σ (σ_{SIE}) in eq. (5). The large solid black squares represent LSD galaxies at $z > 0.4$. The small open triangles at $z = 0.023$ represent the sample of Coma E+S0 galaxies from JFK. Evolutionary trends for a number of recent determinations are also plotted, as solid, dotted, and dashed lines. The thick red lines represent the best linear fit to the SLACS data (*solid*) and to the SLACS+LSD data (*dashed*). The thick blue line summarizes the very similar values found by Treu & Koopmans (2004), Treu et al. (2002, 2005a, 2005b; T02, T05), van der Wel et al. (2004, 2005; vdW04, vdW05). The thick black lines represent measurements for lens samples by van de Ven (2003 vdV03; *dot-dashed*), Rusin et al. (2003, R03; *dotted*) and Rusin & Kochanek (2005; RK05; *dashed*). The thin blue line represent field measurements from Gebhardt et al. (2003; G03; *dashed*). The thin magenta lines represent cluster measurements from van Dokkum et al. (1998; vD98; *dashed*) and Wuyts et al. 2004 (W04; *dotted*). All the lines are based on spectroscopic stellar velocity dispersions, except for vdV03, R03, and RK05.

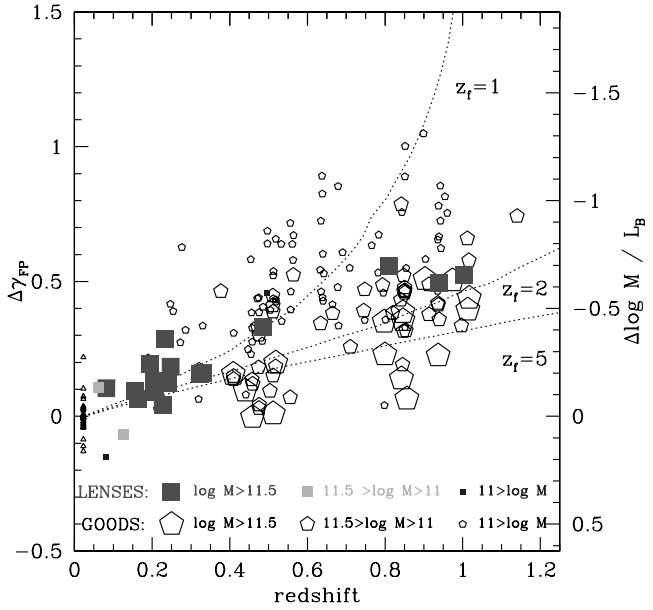

FIG. 7.—Comparison between the evolution of M/L_B for SLACS and LSD lenses (*filled symbols*) and that for field early-type galaxies in the GOODS-N field (from Treu et al. 2005a, 2005b; *open black symbols*). The size of the symbols encodes the effective mass (in solar units). The local reference sample of the Coma Cluster is also shown as small open symbols at $z = 0.023$. Tracks corresponding to passive evolution of a single-burst stellar population formed at $z = 1$, 2, and 5 are overlaid for guidance (see Treu et al. 2005b for a description of the models). Note that most lenses are in the highest effective mass bin and the evolution of the GOODS-N field lenses depends strongly on the effective mass. [*See the electronic edition of the Journal for a color version of this figure*.]

the error bars. Adopting σ_{SIE} in equation (5) changes the linear fit to the evolution of the M/L_B of the SLACS lenses to $d\log(M/L_B)/dz = -0.73 \pm 0.08$, i.e., less than the uncertainty. The change is somewhat larger for the LSD lenses, perhaps due to the larger relative importance of the lens environment or large-scale structure along the line of sight, as discussed in § 3.2. Extending the fit based on σ_{SIE} to the SLACS+LSD lenses yields $d\log(M/L_B)/dz = -0.66 \pm 0.02$.

4.1. *Discussion and Comparison with Previous Work*

In Figure 6 the evolution measured for the SLACS and LSD lenses is compared to the best-fit values found by previous studies (see the caption to Fig. 6 for a key to the lines). We emphasize that such comparisons should be taken with caution given the different selection criteria for the various samples and the importance of accounting for selection effects to interpret the evolution of the FP (see discussions in Treu et al. 2001a, 2002, 2005b).

Within the error bars, the SLACS+LSD evolution in M/L agrees with the average evolutionary rate found for nonlens field early-type galaxies by the most recent and comprehensive studies. In comparison with studies of other samples of lens galaxies, however, the SLACS+LSD sample yields a faster evolutionary rate than the Rusin et al. (2003; -0.56 ± 0.04) and Rusin & Kochanek (2005; -0.50 ± 0.19) studies.[11] The discrepancy is reduced if only SLACS lenses are considered, although it must be kept in mind that SLACS lenses are selected to be red and quiescent and therefore biased toward slower evolution. Alternatively, the discrepancy is reduced if σ_{SIE} is adopted for the SLACS+LSD lenses, perhaps indicating that part of the reason for this mild discrepancy lies in the isothermal approximation for the highest redshift systems.

In conclusion, noting the various selection effects and still relatively large uncertainties and small numbers at high z for the lens samples, no convincing evidence is found that the evolution of the fundamental plane is different for lens and nonlens E+S0 galaxies. Possible differences are best investigated in the context of the mass dependency (downsizing) reported for nonlens samples. This is illustrated in Figure 7, in which we compare the evolution of the FP for SLACS+LSD lenses to that found by Treu et al. (2005a, 2005b) for a sample of 141 field E+S0 galaxies in the GOODS-N field. The vast majority of the lenses have masses above $10^{11.5}\ M_\odot$ and follow approximately the evolutionary path observed for field E+S0 galaxies in the same mass range, i.e., passive evolution of an old stellar population formed at $z \sim 2$ with limited amounts of stars formed in secondary bursts at lower redshift. In order to avoid duplicating previous work, we do not discuss this in more detail or more quantitatively, referring instead to the extended discussion and analysis in Treu et al. (2005b).

A possible hint of difference is found when comparing the M/L of the three high-redshift LSD lenses to that of the

[11] A measure of the systematic uncertainties related to the methodology is given by the van de Ven et al. (2003) reanalysis of the same sample of lenses, which gives -0.62 ± 0.13.

high-mass E+S0 galaxies in GOODS. The three lenses are in the lower M/L part of the distribution. According to a K-S test, the probability that the three LSD lenses are drawn from the same distribution as that of the massive E+S0 galaxies is 6%. The lowest M/L of the three lenses is HST 1417, which has been known for quite some time to show fast evolution (Ohyama et al. 2002; Gebhardt et al. 2003; Treu & Koopmans 2004; van der Wel et al. 2004) and happens to be the least massive of the three. This possible difference must be taken with great care given the extremely different selection criteria and their importance in interpreting the FP (e.g., Treu et al. 2005a, 2005b). In particular, the spectroscopic limit for LSD was not as deep as it was for the GOODS study, possibly imposing a more stringent upper limit on the measurable M/L. Given the small number statistics involved, we do not attempt to quantify the significance of this difference any further, but we await the collection of a larger sample (suitable targets are rapidly becoming available, e.g., Cabanac et al. 2005). We conclude by emphasizing that lenses occupy the same FP as normal E+S0 (§ 3.1), and they have exactly the same M/L for a given M (Fig. 3, *top*). Therefore, their distribution inside the FP and any selection in σ is irrelevant to the determination of the evolution of M/L.

5. SUMMARY AND CONCLUSIONS

We have performed two-dimensional surface photometry on the *HST* ACS images of 15 lens early-type galaxies identified by SLACS. As described in Paper I (Bolton et al. 2006) the lenses are selected from the luminous red galaxy and main galaxy sample of the SDSS database with quiescent spectra, i.e., equivalent width of Hα < 1.5 Å. In combination with stellar velocity dispersions from the SDSS database, we have constructed the fundamental plane of lens galaxies and measured its evolution with redshift. We have compared the measured stellar velocity dispersion with the velocity dispersion of the singular isothermal ellipsoid that best fits the lensing geometry (see Paper III) to study the homogeneity of lens galaxies and the accuracy of the isothermal approximation to measure the evolution of the FP of lens galaxies. The main results can be summarized as follows:

1. SLACS lenses define a fundamental plane correlation over almost a decade in effective radii. The lenses are typically brighter than local early-type galaxies for a given velocity dispersion and effective radius, consistent with lower mass to light ratios, i.e., younger stellar populations at $z = 0.06$–0.33, than today.

2. After correction for evolution of the stellar populations, the SLACS lenses fall on the FP of early-type galaxies in the local universe. The edge-on projection of the FP of SLACS lenses is consistent with that of local galaxies within the errors. In contrast, SLACS lenses occupy a relatively small portion of the plane, concentrating along the border of the so-called zone of avoidance of local early-type galaxies. We show that this is the result of our selection procedure focused on the systems with the highest velocity dispersion. Accounting for the selection procedure, the distribution of distances from the zone of avoidance is indistinguishable from that of the SDSS parent samples (main sample and LRG). We conclude that the SLACS lenses are a fair sample of high velocity dispersion ($\sigma \gtrsim 240$ km s^{-1}) early-type galaxies.

3. The ratio between the central stellar velocity dispersion (σ) and velocity dispersion of the singular isothermal ellipsoid ($\sigma_{\rm SIE}$) that best fits the lensing geometry is found to be $\langle f_{\rm SIE}\rangle = 1.010 \pm 0.017$, with an rms scatter of 0.065. The isothermal approximation for the SLACS lenses works better than that for the LSD sample of five galaxies at higher redshifts ($\langle f_{\rm SIE}\rangle = 0.87$, with rms scatter 0.08). If this redshift dependency is confirmed by larger and homogeneously selected samples at higher redshift, possible explanations include an intrinsic change in the properties of early-type galaxies with cosmic time or simply by an increased contribution of external convergence, resulting from group or clusters associated with the lens or large-scale structures along the line of sight.

4. Interpreting the evolution of the FP in terms of evolution of the stellar populations, the effective M/L of SLACS lenses evolves as $d\log(M/L_B)/dz = -0.69 \pm 0.08$, with an rms scatter of 0.11. Adding the five galaxies from the LSD sample, the best-fit evolutionary rate changes to -0.76 ± 0.03, leaving the scatter unchanged. The evolutionary rate changes within the error if $\sigma_{\rm SIE}$ is used to construct the FP instead of σ.

We now briefly discuss these results in terms of their implications for our understanding of the formation and evolution of early-type galaxies.[12] From the point of view of stellar populations, we find that the SLACS lenses have a mostly old stellar population, with at most a small (<10%) contribution of stellar mass accreted at $z < 1$. This is in agreement with what is found (e.g., Treu et al. 2005a, 2005b) for nonlens early-type galaxies of comparable mass ($\langle\sigma\rangle = 279$; rms scatter of 45 km s^{-1}). This conclusion is unlikely to be significantly biased by our selection criterion against Hα emission, since at the redshifts of the current SLACS sample ($\langle z\rangle = 0.19$), emission lines are not frequent even in morphologically selected samples (e.g., Treu et al. 2002).

Concluding that most stars are old, however, does not answer the question of how and when the stars and dark matter are assembled. An often-invoked mechanism for the assembly of massive early-type galaxies (e.g., Khochfar & Burkert 2003) involves the so-called dry mergers, i.e., mergers that do not involve a significant amount of cold gas and hence are not associated with star formation (see Bell et al. 2006 and van Dokkum 2005 for recent results and discussions). Since the stars in merging galaxies are already old and the dynamical timescales for mergers are rather short (a few hundred million years), dry mergers provide an efficient way to assemble large amounts of old stars with little remnants.

However, the old stellar ages are only one of the observational tests of the dry mergers hypothesis. The tight scatter of empirical scaling laws such as the fundamental plane and the black hole mass–σ relation must also be explained under this scenario. Numerical simulations show that plausible configurations of major dry mergers preserve the tightness of the FP, i.e., if two galaxies start on the FP they also end up on the FP (Nipoti et al. 2003; Gonzalez-Garcia & van Albada 2003; Boylan-Kolchin et al. 2005), with an edge-on thickness comparable to that observed. In contrast, other scaling laws, such as the Kormendy and Faber-Jackson relationships and the black hole mass σ relationship, are not naturally preserved by dry mergers (Nipoti et al. 2003). A substantial amount of dissipation seems to be necessary to preserve those (e.g., Kazantzidis et al. 2005).

The observations present here provide a new series of tests for this hypothesis. First, we measure the distribution of early-type galaxies within the FP: this also should be reproduced by a successful formation mechanism. At the moment there is no good explanation for the zone of avoidance, nor does it appear clear whether dry mergers alone can populate the right portion of the plane (as suggested perhaps by the difficulties in reproducing the Kormendy and Faber-Jackson relation). It is possible that dissipation may end up to be necessary to move the objects

[12] To avoid duplications within the series, the main discussion is left for Paper III.

toward higher concentration, against the boundary of the zone of avoidance (see Bender et al. 1992).

Second, the proposed mechanism must also explain the distribution of mass *inside* each galaxy. Our study shows very clearly that, at these scales (typically $R_e/2$), early-type lens galaxies are well approximated by singular isothermal ellipsoids (see also KT and Paper III). Not only does this mass-density profile differ significantly from cosmologically motivated ones (e.g., Navarro et al. 1997; Moore et al. 1998), but it also requires a significant amount of fine-tuning between the distribution of luminous and dark matter (the bulge-halo conspiracy). It has been suggested that the total mass-density profile can act as a "dynamical attractor" for collisionless particles (i.e., stars and dark matter; Loeb & Peebles 2003; Gao et al. 2004) in a similar way to the close-to-isothermal profiles obtained for (incomplete) violent relaxation scenarios (e.g., van Albada 1982). Our measurements provide a quantitative test for this idea. From the point of view of dry mergers, the close-to-isothermal mass-density profile raises two problems. The first is whether such a property is preserved during dry mergers. Assuming that this is the case, the second problem is how the progenitors got their initial mass-density profile. Simulations of dry mergers typically start with input galaxies already "dense" and close to isothermal, but—as we argue in Paper III—this process cannot be traced back ad infinitum. A different process—perhaps gas-rich mergers—appears to be needed at some point to create these high-concentration objects. This brings us back to the main unanswered question: what is the origin of the bulge-halo conspiracy?

We thank the referee for a careful and insightful report that significantly improved the paper. We are grateful to Luca Ciotti, Barbara Lanzoni, and Simon White for useful conversations. We acknowledge financial support from *HST* grants (STScI-AR-09222; STScI-GO-10174). T. T. acknowledges support from NASA through Hubble Fellowship grant HF-01167.1 and thanks UCLA for being such a welcoming and stimulating Hubble Fellowship host institution during the initial phases of this project. The work of L. A. M. was carried out at the Jet Propulsion Laboratory, California Institute of Technology, under a contract with NASA. This project would not have been feasible without the extensive and accurate database provided by the Digital Sloan Sky Survey (SDSS). Funding for the creation and distribution of the SDSS Archive has been provided by the Alfred P. Sloan Foundation, the Participating Institutions, the National Aeronautics and Space Administration, the National Science Foundation, the Department of Energy, the Japanese Monbukagakusho, and the Max Planck Society. The SDSS Web site is http://www.sdss.org. The SDSS is managed by the Astrophysical Research Consortium (ARC) for the Participating Institutions. The Participating Institutions are the University of Chicago, Fermilab, the Institute for Advanced Study, the Japan Participation Group, Johns Hopkins University, the Korean Scientist Group, Los Alamos National Laboratory, the Max Planck Institute for Astronomy, the Max Planck Institute for Astrophysics, New Mexico State University, University of Pittsburgh, University of Portsmouth, Princeton University, the United States Naval Observatory, and the University of Washington.

REFERENCES

Bell, E. F., et al. 2006, ApJ, 640, 241
Bender, R., Burstein, D., & Faber, S. M. 1992, ApJ, 399, 462
———. 1993, ApJ, 411, 153
Bender, R., Saglia, R. P., Ziegler, B., Belloni, P., Greggio, L., Hopp, U., & Bruzual, G. 1998, ApJ, 493, 529
Bernardi, M., et al. 2003, AJ, 125, 1866
Bertin, G., Ciotti, L., & Del Principe, M. 2002, A&A, 386, 149
Blanton, M., et al. 2003, AJ, 125, 2348
Bohlin, R. C., & Gilliland, R. L. 2004, AJ, 127, 3508
Bolton, A., Burles, S. M., Koopmans, L. V. E., Treu, T., & Moustakas, L. M. 2005, ApJ, 624, L21
———. 2006, ApJ, 638, 703 (Paper I)
Bolton, A., Burles, S., Schlegel, D. J., Eisenstein, D. J., & Brinkmann, J. 2004, AJ, 127, 1860
Boylan-Kolchin, M., Ma, C.-P., & Quataert, Q. 2005, MNRAS, 362, 184
Cabanac, R., et al. 2005, A&A, 436, L21
Ciotti, L., Lanzoni, B., & Renzini, A. 1996, MNRAS, 282, 1
Cowie, L. L., Songaila, A., Hu, E. M., & Cohen, J. G. 1996, AJ, 112, 839
Dalal, N., & Watson, C. 2004, ApJ, submitted (astro-ph/0409483)
de Lucia, G., Springel, V., White, S. D. M., Croton, D., & Kauffmann, G. 2006, MNRAS, 366, 499
di Serego Alighieri, S., et al. 2005, A&A, 442, 125
Djorgovksi, S. G., & Davis, M. 1987, ApJ, 313, 59
Dressler, A., Lynden-Bell, D., Burstein, D., Davies, R. L., Faber, S. M., Terlevich, R., & Wegner, G. 1987, ApJ, 313, 42
Eisenstein, D. J. 2001, AJ, 122, 2267
Faber, S. M., Dressler, A., Davies, R. L., Burstein, D., & Lynden-Bell, D. 1987, in Nearly Normal Galaxies, ed. S. M. Faber (New York: Springer), 175
Fassnacht, C. D., & Lubin, L. 2002, AJ, 123, 627
Fassnacht, C. D., et al. 2005, in IAU Symp. 225, Gravitational Lensing Impact on Cosmology, ed. Y. Mellier & G. Meylan (Cambridge: Cambridge Univ. Press), 311
Ferrarese, L., & Merritt, D. 2000, ApJ, 539, L9
Fritz, A., Ziegler, B. L., Bower, R. G., Smail, I., & Davies, R. L. 2005, MNRAS, 358, 233
Gao, L., Loeb, A., Peebles, P. J. E., White, S. D. M., & Jenkins, A. 2004, ApJ, 614, 17
Gavazzi, G. 1993, ApJ, 419, 469
Gebhardt, K., et al. 2000, ApJ, 539, L13
———. 2003, ApJ, 597, 239
Gonzalez-Garcia, A. C., & van Albada, T. S. 2003, MNRAS, 342, L36
Hamabe, M., & Kormendy 1987, in IAU Symp. 127, Structure and Dynamics of Elliptical Galaxies, ed. P. T. de Zeeuw (Dordrecht: Reidel), 379
Hernquist, L. 1990, ApJ, 356, 359
Holden, B., et al. 2005, ApJ, 620, L83
Holder, G. P., & Schechter, P. L. 2003, ApJ, 589, 688
Huchra, J. P., Gorenstein, M., Kent, S., Shapiro, I., Smith, G., Horine, E., & Perley, R. 1985, AJ, 90, 691
Jorgensen, I., Franx, M., & Kjaergaard, P. 1992, A&AS, 95, 489
———. 1993, ApJ, 411, 34
———. 1995, MNRAS, 276, 1341
———. 1996, MNRAS, 280, 167
Juneau, S., et al. 2005, ApJ, 619, L135
Kazantzidis, S., et al. 2005, ApJ, 623, L67
Keeton, C. R., & Zabludoff, A. I. 2004, ApJ, 612, 660
Kelson, D. D., Illingworth, G. D., van Dokkum, P. G., & Franx, M. 2000, ApJ, 531, 184
Kelson, D. D., van Dokkum, P. G., Franx, M., Illingworth, G. D., & Fabricant, D. G. M. 1997, ApJ, 478, L13
Khochfar, S., & Burkert, A. 2003, ApJ, 597, L117
Kochanek, C. S. 2002, ApJ, 578, 25
Kochanek, C. S., et al. 2000, ApJ, 543, 131
———. 2006, ApJ, 640, in press (astro-ph/0508070)
Koopmans, L. V. E., & Treu, T. 2002, ApJ, 568, L5
———. 2003, ApJ, 583, 606
Koopmans, L. V. E., Treu, T., Bolton, A. S., Burles, S., & Moustaks, L. A. 2005, ApJ, submitted (astro-ph/0601628) (Paper III)
Koopmans, L. V. E., Treu, T., Fassnacht, C. D., Blandford, R. D., & Surpi, G. 2003, ApJ, 599, 70
Krist, J. 2005, The TinyTim User's Guide, Version 6.03, http://www.stsci.edu/software/tinytim/tinytim.html
Lanzoni, B., Ciotti, L., Cappi, A., Tormen, G., & Zamorani, G. 2004, ApJ, 600, 640
Loeb, A., & Peebles, P. J. E. 2003, ApJ, 589, 29
McIntosh, D., et al. 2005, ApJ, 632, 191
Moore, B., Governato, F., Quinn, T., Stadel, J., & Lake, G. 1998, ApJ, 499, L5
Moran, S. M., Ellis, R. S., Treu, T., Smail, I., Dressler, A., Coil, A., & Smith, G. P. 2005, ApJ, 634, 977
Navarro, J., Frenk, C. S., & White, S. D. M. 1997, ApJ, 490, 493
Nipoti, C., Londrillo, P., & Ciotti, L. 2003, MNRAS, 342, 501
Ohyama, Y., et al. 2002, AJ, 123, 2903
Pahre, M. A. 1998, Ph.D. thesis, Caltech

Peng, C., Ho, L. C., Impey, C. D., & Rix, H.-W. 2002, AJ, 124, 266
Rusin, D., & Kochanek, C. S. 2005, ApJ, 623, 666
Rusin, D., et al. 2003, ApJ, 587, 143
Sheth, R., et al. 2003, ApJ, 594, 1810
Strauss, M. A., et al. 2002, AJ, 124, 1810
Treu, T., Ellis, R. S., Liao, T. X., & van Dokkum, P. G. 2005a, ApJ, 622, L5
Treu, T., & Koopmans, L. V. E. 2002a, ApJ, 575, 87
———. 2002b, MNRAS, 337, L6
———. 2003, MNRAS, 343, L29
———. 2004, ApJ, 611, 739
Treu, T., Stiavelli, M., Bertin, G., Casertano, C., & Møller, P. 2001a, MNRAS, 326, 237
Treu, T., Stiavelli, M., Casertano, C., Møller, P., & Bertin, G. 1999, MNRAS, 308, 1037
———. 2002, ApJ, 564, L13
Treu, T., Stiavelli, M., Møller, P., Casertano, C., & Bertin, G. 2001b, MNRAS, 326, 221
Treu, T., et al. 2005b, ApJ, 633, 174
Trujillo, I., Burkert, A., & Bell, E. 2004, ApJ, 600, L39
van Albada, T. S. 1982, MNRAS, 201, 939
van Albada, T. S., Bertin, G., & Stiavelli, M. 1995, MNRAS, 276, 1255
van de Ven, G., van Dokkum, P. G., & Franx, M. 2003, MNRAS, 344, 924
van der Wel, A., Franx, M., van Dokkum, P. G., & Rix, H.-W. 2004, ApJ, 601, L5
van der Wel, A., Franx, M., van Dokkum, P. G., Rix, H.-W., Illingworth, G. D., & Rosati, P. 2005, ApJ, 631, 145
van Dokkum, P. G. 2005, AJ, 130, 2647
van Dokkum, P. G., & Ellis, R. S. 2003, ApJ, 592, L53
van Dokkum, P. G., & Franx, M. 1996, MNRAS, 281, 985
van Dokkum, P. G., Franx, M., Kelson, D. D., & Illingworth, G. D. 1998, ApJ, 504, L17
———. 2001, ApJ, 553, L39
van Dokkum, P. G., & Stanford, S. A. 2003, ApJ, 585, 78
Wuyts, S., van Dokkum, P. G., Kelson, D. D., Franx, M., & Illingworth, G. D. 2004, ApJ, 605, 677
Yee, H. K. C., Hsieh, B. C., Lin, H., & Gladders, M. D. 2005, ApJ, 629, L77